The Cryosphere Discuss., 5, 855–883, 2011
www.the-cryosphere-discuss.net/5/855/2011/
doi:10.5194/tcd-5-855-2011

The Cryosphere Discussions

Ideal climatic variables for the present-day geometry of the Gregoriev Glacier, Inner Tien Shan, Kyrgyzstan, derived from GPS data and energy-mass balance measurements

K. Fujita[1], N. Takeuchi[2], S. A. Nikitin[3], A. B. Surazakov[4], S. Okamoto[1], V. B. Aizen[4], and J. Kubota[5]

[1]Graduate School of Environmental Studies, Nagoya University, Nagoya, Japan
[2]Graduate School of Science, Chiba University, Chiba, Japan
[3]Department of Glacio-Climatology, Tomsk State University, Tomsk, Russia
[4]College of Science, University of Idaho, Moscow, Idaho, USA
[5]Research Institute for Humanity and Nature, Kyoto, Japan

Received: 9 February 2011 – Accepted: 8 March 2011 – Published: 14 March 2011

Correspondence to: K. Fujita (cozy@nagoya-u.jp)

Published by Copernicus Publications on behalf of the European Geosciences Union.

Abstract

We conducted 2 yr (2005–2007) of in situ meteorological and glaciological observations on the Gregoriev Glacier, a flat-top glacier within the Inner Tien Shan, Kyrgyzstan. Differential GPS surveys reveal a vertical surface deletion at the summit of the glacier. Based on snow density data and an energy-mass balance model, we estimate that the annual precipitation and summer mean temperature required to maintain the glacier in the modern state are 289 mm and −3.85 °C at the glacier summit (4600 m above sea level, a.s.l.), respectively. The good agreement between the long-term estimated and observed precipitation at a nearby station in the Tien Shan (292 mm at 3614 m a.s.l. for the period 1930–2002) suggests that the glacier dynamics have been regulated by the long-term average accumulation. The glacier mass-balance, reconstructed based on meteorological data from the Tien Shan station for the past 80 yr, explains the observed fluctuations in glacier extent, particularly the negative mass balance in the 1990s.

1 Introduction

Glaciers are one of the most sensitive indicators of climate change. The evaluation of changes in glacier area and volume has many applications in hydrological modelling and estimations of variability in water resources. Despite the extremely dry climate in central Asia, the Tien Shan holds one of the greatest concentrations of glacier ice in the mid-latitudes, representing a vital source of water for more than 100 million people living in the region.

Glacier dynamics are determined primarily by climate-mediated glacier mass-balance (the net gain or loss of snow and ice). Despite the importance of knowledge on glacier mass-balance variability in terms of regional water resources, regular measurements of glacier mass-balance and other ground-based glaciological data were discontinued in the Tien Shan in 1991. To overcome this lack of data, the extent of

TCD
5, 855–883, 2011

glaciers in this region has been studied using remote sensing data (e.g., Khromova et al., 2003; Aizen et al., 2006, 2007a; Narama et al., 2006; Surazakov and Aizen, 2006; Bolch, 2007; Kutuzov and Shahgedanova, 2009). However, information on glacier variability derived from remote sensing data, which also includes aerial photographs taken in the mid-20th century, is not sufficient to understand the nature of glacier dynamics and its climatic forcing. Long-term observations of climate and glacier mass-balance at several representative glaciers in the Tien Shan were started in 1960 and continued until 1991 (e.g., Golubev, 1976; Konovalov, 1979; Suslov, 1980; Krenke, 1982; Aizen, 1983, 1985; Avsuyk, 1984; Glazirin, 1991), but few mass-balance studies have been undertaken in the past 20 yr. Reconstructions of glacier mass balance, using a mass balance model, are a valid approach to understanding the behaviour of glaciers in the Tien Shan, because long-term climate data are available for the region; however, there have been few studies of this type (Hagg et al., 2005). To reconstruct the mass balance of the Tien Shan glaciers and to understand their threshold for the present-day glacier geometory, we analysed the main climatic variables (precipitation and summer air temperature) observed at the Tien Shan meteorological station, performed in situ meteorological and mass-balance observations at the summit of the Gregoriev Glacier for 2 yr (2005–2007), and considered the results of an energy-mass balance model.

2 Study site, observations, and methods

2.1 Location

The Gregoriev Glacier is an ice-cap type (flat-summit) glacier on the south slope of the Terskey-Alatoo range in the Inner Tien Shan, Kyrgyzstan (41°58′ N, 77°55′ E; Fig. 1). This glacier has been well investigated because of easy access provided by a nearby highway (e.g., Thompson et al., 1993; Nagornov et al., 2006). Changes in air temperature at the glacier summit during the middle of the 20th century have been retrieved from stable water isotopes in ice cores drilled in 1990 and from changes in

TCD
5, 855–883, 2011

borehole temperature (Thompson et al., 1993). Although the thermodynamic state of the glacier has been depicted by a two-dimensional flow-line model, the mass balance as a boundary condition was estimated by a simplified relation based on temperature, precipitation, and altitude (Nagornov et al., 2006).

Figure 1 shows a satellite image of the Gregoriev Glacier taken on 21 August 1980. The area-altitude distribution of the glacier is obtained from recent Landsat ETM+ images (2000 and 2006) that show the glacier extent, and from an SRTM digital elevation model (Jarvis et al., 2008) and ASTER-GDEM (ASTER-GDEM, 2009) for the 50-m altitude band. Temporal change in glacier area is not taken into account in the present analysis.

We conducted in situ observations of the glacier for 2 yr between July 2005 and September 2007, including meteorological observations using an automatic weather station (AWS), surveys using differential GPS (DGPS), and conventional mass-balance measurements using wooden stakes and snow-pits. A surface-to-bedrock ice core (87.46 m deep) was drilled in September 2007. The ice-core is currently being processed and examined for multi-proxy analysis.

2.2 Automatic weather station

An AWS (AANDERAA Data Instruments Inc.) was installed at the summit of the Gregoriev Glacier on 12 July 2005, recording air temperature, relative humidity, wind speed and direction, and downward and upward solar radiation at 30-min intervals. Changes in surface level were measured by two different instruments: an ultra-sonic sensor (AANDERAA) and a photo-diode sensor (KADEC-SNOW, Kona System Co. Ltd). Precipitation was measured by a tipping bucket installed near the terminus (near the DGPS benchmark, BM in Fig. 1). The precipitation gauge was filled with antifreeze (Field Pro Co. Ltd) to avoid water evaporation from the collected snowfalls. Precipitation was only measured for 5 months (August–December 2006) due to battery failure. All variables were compiled to daily values.

TCD
5, 855–883, 2011

2.3 Mass balance calculated using the stake method and snow-pits

Six stakes were installed around the summit of the Gregoriev Glacier on 27 August 2006 for mass balance measurements and surveys of surface flow velocity. We also measured the mass balance and location of one pre-existing stake found during the 2006 survey. Changes in stake heights and AWS data were used to calculate the mass balance between 2006 and 2007. A snow-pit (2–3 m deep) was dug during each visit to the glacier. The stratigraphy and depths of dust layers were recorded along the pit wall, and a density profile was constructed. Snow density data are necessary to convert changes in stake height to water equivalent (w.e.). The depths of dust layers are used to validate the energy-balance model.

2.4 DGPS surveys

Static surveys by a carrier-phase differential Global Positioning System (DGPS; Pro Mark 2 in 2005 and CMC All Star receivers in 2006 and 2007) were performed to measure stake positions on the Gregoriev Glacier in each year. One GPS receiver was installed as a base station at a benchmark near the glacier terminus (white cross in Fig. 1). Only the position of the AWS was surveyed in 2005. The locations of stakes were surveyed in 2006 and 2007, yielding the flow velocities.

Kinematic surveys, using the same DGPS as that described above, were performed on the glacier in 2006 and 2007. Post-processing of DGPS data was performed using Waypoint GrafNav/GrafNet software (NovAtel Inc.) to obtain the relative positions and altitudes of all points on a common Universal Transverse Mercator projection (UTM, zone 43N, WGS-84 reference system). Data processed as being unstable and converging float solutions were excluded from subsequent analyses (representing 0.8% of the data points in 2006 and 1.2% in 2007). The measurement errors obtained using the same instrument in the same manner have previously been reported as 0.1–0.4 m in location and 0.2–0.9 m in altitude (Fujita et al., 2008, 2009).

TCD
5, 855–883, 2011

All the surveyed points (10 023 in 2006 and 12 954 in 2007) were converted to 1-m-resolution digital elevation models (DEMs) by the inverse distance weighting method, whereby the measured points used to obtain the altitude of a grid cell are limited to within the targeted grid cell. Grid cells without a measurement point were excluded from subsequent analyses. Ultimately, we considered 6363 cells for 2006 and 9796 cells for 2007.

2.5 Energy-mass balance model

The energy-mass balance model used in this study calculates the daily heat balance at the glacier surface, including the radiation balance, sensible and latent turbulent heat fluxes, heat conduction into the glacier, and mass balance consisting of snow accumulation, melt, refreezing, and evaporation, as follows (Fujita and Ageta, 2000; Fujita et al., 2007):

$$\max[Q_M;0] = (1-\alpha)\,R_S + R_L - \min\left[\sigma T_S^4;315.6\right] + Q_S + E_V\,l_e + Q_G \quad (1)$$

Heat for melting (Q_M) is obtained if the right-hand side of the equation is greater than zero. Absorbed short-wave radiation is calculated from the surface albedo (α) and downward short-wave radiation (R_S). Downward long-wave radiation (R_L) is calculated from the air temperature, relative humidity, and the ratio of downward short-wave radiation to that at the top of the atmosphere, using an empirical scheme (Fujita and Ageta, 2000). Upward long-wave radiation is obtained from the Stefan-Boltzmann constant (σ) and the surface temperature in Kelvin (T_S), assuming a black body for the snow/ice surface. A melting surface (0 °C surface temperature) releases upward long-wave radiation of 315.6 (W m^{-2}). Sensible (Q_S) and latent ($E_V\,l_e$) turbulent heat fluxes are obtained by bulk methods. The latent heat for evaporation of water or ice (l_e) is determined from the surface temperature. Conductive heat into the glacier ice (Q_G) is obtained by calculating the temperature profile of the snow layer and/or glacier ice. All heat components are positive when fluxes are directed toward the surface. Mass

TCD
5, 855–883, 2011

balance (B) at any location on the glacier is calculated as follows:

$$B = Ca - Q_M/l_m + E_V + R_F \quad (2)$$

Solid precipitation (Ca, positive sign), which is determined along with air temperature, is equivalent to accumulation over the glacier. Mass is removed from the glacier as meltwater (Q_M/l_m, positive sign) and evaporation (E_V, negative sign). l_m is the latent heat for melting ice. Some of the meltwater is fixed to the glacier by refreezing (R_F, positive sign) if the glacier ice is cold enough (Fujita et al., 1996). The refreezing amount is calculated in the model by considering the conduction of heat into glacier ice and the presence of water at the interface between the snow layer and glacier ice (Fujita and Ageta, 2000). Also considered is refreezing during winter and shorter cooling events. Special attention is paid to the treatment of the surface albedo (α) because it varies enormously in space and time, even for a single glacier (the albedo declines down a glacier and during the course of the melt season). The albedo in the model was calculated according to the surface snow density, which changes with snow compaction. The albedo of bare ice was set to 0.19, as observed in 2006. Detailed schemes for the entire model have been described by Fujita and Ageta (2000) and Fujita et al. (2007), and the albedo and snow densification schemes have been described by Fujita (2007).

2.6 Long-term data

To reconstruct the long-term mass balance, it is necessary to prepare a set of daily meteorological variables, such as air temperature, precipitation, solar radiation, relative humidity, and wind speed. Monthly air temperature and precipitation data recorded at the Tien Shan station (41°55′ N, 78°14′ E; 3614 m a.s.l.; 27 km from the glacier) are used for the period 1930–2002. Because gridded pentad (5-day average) precipitation is available from 1979, we generated daily air temperature and precipitation for the

TCD
5, 855–883, 2011

period 1979–2002, as follows:

$$T_{z,\,\mathrm{day}} = T_{\mathrm{ncep,\,day}} - T_{\mathrm{ncep,\,mon}} + T_{\mathrm{ts,\,mon}} - \Gamma_{\mathrm{day}}\,(z - 3614)$$
$$P_{\mathrm{day}} = \frac{P_{\mathrm{gpcp,\,day}}}{P_{\mathrm{gpcp,\,mon}}}\,P_{\mathrm{ts,\,mon}} \qquad (3)$$

where T and P denote air temperature and precipitation, respectively; $T_{z,\,\mathrm{day}}$ is the daily air temperature at a given altitude (z); and the subscripts ncep, gpcp, day, mon, and ts denote NCEP/NCAR reanalysis data (Kalnay et al., 1996), GPCP precipitation data (Adler et al., 2003), daily and monthly values, and data from the Tien Shan station, respectively. The lapse rate of air temperature (Γ_{day}, expressed as an absolute value) is estimated from geopotential heights and air temperatures at 500 and 600 hPa, from the NCEP/NCAR reanalysis dataset. Because data at the Tien Shan station are unavailable after 2003, we use the relations between reanalysis datasets and data from the Tien Shan station averaged for each month, for the period 1979–2002 ($\left(-T_{\mathrm{ncep,\,mon}} + T_{\mathrm{ts,\,mon}}\right)_{1979-2002}$ for air temperature and $\left(P_{\mathrm{ts,\,mon}}/P_{\mathrm{gpcp,\,mon}}\right)_{1979-2002}$ for precipitation). Daily values of solar radiation, relative humidity, and wind speed are modified for the glacier (see below for details) for the period 1979–2007. For the period 1930–1978, we estimated the daily air temperature and precipitation in the same manner as the Eq. (3), but iterative calculations were performed using 29 seasonal patterns (1979–2007), meaning that the averaged mass balance profile is obtained for each year, because the seasonality of meteorological variables has a marked effect on the mass balance (Fujita, 2008). The other daily variables (solar radiation, relative humidity, and wind speed) for the period 1979–2007 were used for the iterative calculation.

TCD
5, 855–883, 2011

3 Results and discussion

3.1 Observed and gap-filled meteorological data

Because the AWS records were occasionally interrupted due to battery problems, we estimated missing data by linear regression equations established between observed data and the modified reanalysis datasets mentioned above. Table 1 summarizes the parameters used in the regression equations and the correlation coefficients. A marked seasonality yields high correlation coefficients for air temperature and solar radiation. Although wind speed and relative humidity show weaker or insignificant correlations, these variables are less important in calculating the heat balance because of low air pressure at high elevations (Fujita and Ageta, 2000). Pentad precipitation shows a significant correlation, even between point observations and gridded data. We finally established daily variables for the 2-yr observation period, from July 2005 to September 2007 (Fig. 2). These variables were used as input for validation calculation.

3.2 Flow field and net balance required to maintain the glacier in the modern state

Repeated surveys enabled calculation of the flow velocity at the summit of the Gregoriev Glacier (Fig. 3 and Table 2). The lowest stake (i.e., the pre-existing stake) was found during the 2006 survey and was presumably installed during a previous campaign. The locations of the AWS and Stake 3 show small amounts of horizontal movement (dH in Table 2), thereby guaranteeing undisturbed climatic signals in ice cores from this site. Vertical changes in the surface elevation (dSF in Table 2) are slightly positive for the period 2006–2007. When the surface net balance is taken into account (dSA in Table 2), however, a given fixed point for each stake shows a marked lowering (dVD in Table 2). This vertical depletion reflects vertical dynamics throughout the glacier and the slope along the flow line. If horizontal movements are sufficiently small (e.g., AWS and Stake 3), vertical depletion represents the net balance

TCD
5, 855–883, 2011

required to maintain the present-day glacier geometry. We obtained an averaged depletion of $0.53 \pm 0.01\,\mathrm{m\,yr^{-1}}$ from the AWS site. The average surface snow density was $451 \pm 46\,\mathrm{kg\,m^{-3}}$ (calculated from three snow-pits dug every survey); thus, the net accumulation was $238 \pm 27\,\mathrm{mm\,w.e.\,yr^{-1}}$ (Table 3). The precipitation amount required to maintain the present-day glacier geometry can be determined if we know the mass loss by evaporation, which is obtained by model calculations (see below).

3.3 Changes in elevation of the glacier surface

We calculated changes in the surface elevation of the Gregoriev Glacier by comparing the 1-m DEMs constructed in 2006 and 2007 (Figs. 1 and 4a). The elevation difference was calculated at a point for which elevation data were available for both years. The elevation changes calculated at 1-m resolution are averaged to 15-m resolution for better visibility (Fig. 1) and are shown for the 50-m altitude band (Fig. 4a). The elevation changes show a reasonable altitudinal profile, except for the lowermost part of the glacier, where bedrock is probably encountered. We extrapolated the elevation change at the lowermost part of the glacier using the data at 4300 and 4250 m a.s.l. Considering the area-altitude distribution (Fig. 4a), the area-averaged specific mass balance (SMB) is −0.36 m w.e. for the period 2006–2007 (Table 4).

3.4 Validation of the energy-balance model and impact of dust events

We performed mass balance calculations for the period 2005–2007 using the energy-mass balance model and the gap-filled meteorological data, as mentioned above. Figure 5 compares the calculated changes in albedo and relative surface height at the glacier summit with observed data. Although the modelled surface appears to follow the observed surface in the first year, a large depletion of the surface in August 2006 was not reproduced by the model, meaning that the inconsistency between observations and calculations increased in the second year (thin line in Fig. 5b). In contrast, the observed surface albedo showed a large reduction when the surface was depleted

TCD
5, 855–883, 2011

in August 2006 (Fig. 5a). The presence of a dust layer observed at a depth of 6.5 cm in the snow-pit excavated in August 2006 (red diamond in Fig. 5b) indicates that a dust-fall event darkened the snow surface, causing a marked lowering of the surface due to melting. Therefore, we darkened the surface in the calculation using the dust-tracking scheme established by Fujita (2007), in which the position of dust is traced by considering snow compaction. The albedo of a dusty surface is assumed to be 0.55, based on observations (Fig. 5a). The dust run reproduces a reduction in albedo (Fig. 5a) and the consequent surface lowering (Fig. 5b). The change in surface level during the second year is therefore consistent with that observed (thick black line in Fig. 5b). A deeper dust layer observed in September 2007 supports the representativeness of the traced dust layer (red diamonds and thick brown line in Fig. 5b). Another, shallower dust layer observed in the shallower part of the snow-pit in September 2007 should have been formed during March–April 2007, as suggested by the stable surface position and lower albedo in the spring of 2007.

An altitudinal mass balance profile and the SMB (−0.41 m w.e.) of the calculation are consistent with the DGPS surveys (Fig. 4b and Table 4). However, the profile of change in surface height should be smoother than that of the mass balance because the emergence velocity modified the shape of the glacier. In other words, the glacier surface is thinning in the upper accumulation area and being uplifted in the lower ablation area, in order to maintain its overall shape. If the glacier is in a steady state, the change in surface elevation should be zero at all altitudes. The relaxation effect associated with glacier flow is equivocal, probably because the surveys were conducted in seasons of rapid melting and accumulation, when the glacier surface shows a marked change due to snowfall, dust fall, or high-temperature events. In addition, data on the change in surface elevation over a period of just 1 yr would obscure the effect of glacier flow on geometry.

Mass balance profiles obtained for the control and dust runs for the period 2005–2006 show a significant difference around the middle part of the glacier (4300–4400 m a.s.l.; Fig. 4b). Despite the significant surface lowering due to dust fall in the

TCD
5, 855–883, 2011

calculation (Fig. 5b), meltwater was refrozen within the cold snow pack around the summit of the glacier. At the lower part of the glacier, on the other hand, dust fall did not affect the mass balance because of the small amount of surface snow, even in the control run. Dust fall has a strong effect on the timing of appearance of an ice surface with a low albedo (0.19) on the surface, thereby affecting the mass balance around the middle part of the glacier. The dusted SMB (−1.60 m w.e.) was much more negative than that of the control run (−1.34 m w.e.; Table 4).

3.5 Climate required to maintain the modern state of the glacier

Using the energy-mass balance model and the estimated meteorological variables (see above), evaporation at the summit of the glacier for the period 1979–2007 was calculated to be 51 ± 8 mm w.e. yr^{-1} (Table 3). Annual precipitation, which is equivalent to the sum of net balance and evaporation under a condition of no discharge, was 289 ± 35 mm yr^{-1}, which is surprisingly consistent with the long-term annual precipitation recorded at the Tien Shan station (292 ± 102 mm yr^{-1} for the period 1930–2002) (Table 3). In other words, this consistency indicates that the long-term precipitation amount is a threshold value in maintaining the present-day glacier geometry (specific mass balance of zero) and has regulated the glacier dynamics.

If annual precipitation is constrained by the ideal precipitation, the air temperatures required to maintain the present-day glacier geometry can be obtained from iterative calculations, in which annual air temperature is varied systematically. In this way, we obtained an ideal summer mean air temperature (average of June–August, JJA) at the summit of the glacier (4600 m a.s.l.) of -3.85 ± 0.60°C (Table 3). Variability in temperature is derived from variability in ideal precipitation (± 35 mm) and the fact that the 29 seasonal patterns (1979–2007) show different seasonalities in the relevant variables. Figures 4c and 6 show an ideal mass balance profile, and the JJA temperature and annual precipitation for the present-day glacier geometry, respectively.

Our analysis did not consider glacier dynamics. The altitude-area distribution of the glacier is assumed to have been constant during the analysis period, whereas

TCD
5, 855–883, 2011

shrinkage of the glacier has been reported based on remotely sensed data (e.g., Aizen et al., 2006, 2007a; Narama et al., 2006; Kutuzov and Shahgedanova, 2009) (Fig. 1). An increase in the area of the lower part of the glacier would result in a reduced SMB, corresponding to a cooler ideal temperature condition for the present-day glacier geometry. If the lower area (3900–4100 m a.s.l.) is assumed to be larger than the present-day area by 0.71 km^2 (10% of the present-day total area), the ideal JJA temperature should be cooler by 0.18 °C, which is less than the uncertainty due to the seasonality of meteorological data (0.60 °C).

3.6 Mass balance reconstruction

We calculated the long-term mass balance for the past 80 yr (Fig. 6). The calculated SMB and equilibrium line altitude (ELA) are consistent with observation data for the Karabatkak Glacier, located on the northern slopes of the same mountain range as that considered in the present study (42°09′ N, 78°16′ E; 35 km from Gregoriev Glacier; data from Dyrugerov, 2002). The calculation results are also supported by observation data for the Gregoriev Glacier (open diamonds in Fig. 6c; data from Dyrugerov, 2002). The ELA of the Karabatkak Glacier appears to be 500 m lower than that of the Gregoriev Glacier (Fig. 6d), because the average accumulation at the former is about 2.5 times larger than that at the latter. However, fluctuations in SMB and ELA calculated for the Gregoriev Glacier are consistent with those for the Karabatkak Glacier, suggesting that the climatic variables which affect the glacier mass balance (i.e., precipitation and summer temperature) show similar fluctuations throughout this region, whereas the baselines of annual precipitation differ between the two glaciers.

We also confirmed the influence of constant glacier area in the assumption on the resulting mass balance, in the same manner as that for the ideal JJA temperature (as described above). If we assume the lower area (3900–4100 m a.s.l.) to be larger than the present-day size by 0.71 km^2 (10% of the present-day total area), the specific mass balance is more negative by 0.15 m w.e., which is the average for the calculation period, while the average uncertainty due to different seasonal patterns of meteorological

TCD
5, 855–883, 2011

inputs is 0.47 m w.e. This result indicates that a change in glacier extent has a smaller impact on the SMB than does uncertainty due to seasonal patterns (Fig. 6c).

The correlation coefficients between mass balance and monthly mean air temperature are greater (worse) than −0.675 (July). The strongest four correlations are obtained for the averages of JJA (−0.732), JA (July–August, −0.719), MJJAS (May–September, −0.718), and JJ (June–July, −0.715). The correlation coefficients between mass balance and monthly precipitation are smaller than 0.498 (June); the strongest four correlations are obtained for annual data (0.678), MJJA (May–August, 0.672), MJJAS (0.671), and JJA (0.655). Therefore, we conclude that annual variability in the mass balance of the Gregoriev Glacier has been strongly influenced by annual variability in JJA temperature and annual precipitation.

By comparing the JJA temperature, annual precipitation, ELA, and mass balance with the ideal conditions (−3.85 °C as JJA temperature at the glacier summit and 289 mm as annual precipitation), we can investigate which variables have controlled the glacier mass balance in each decade. Warm conditions that were occasionally observed before 1980 appear to be the main cause of negative mass balances. After 1980, in contrast, a marked reduction in precipitation resulted in accelerated mass loss of the glacier for two decades. Despite a recovery in annual precipitation after the 1990s, warm temperatures (above those of the ideal condition) appear to have forced wasting of the ice mass of the glacier. Kutuzov and Shahgedanova (2010) reported accelerated shrinkage of glacier extent in this region based on remote sensing data and the climate records of the Tien Shan station, but the present calculations yield greater detail with respect to the behaviour of glacier mass balance over the past 80 yr.

4 Conclusions

We obtained the ideal accumulation amount required to maintain the present-day geometry of the Gregoriev Glacier (a flat-top glacier in the Inner Tien Shan, Kyrgyzstan) based on differential GPS surveys that detected the depletion rate of stakes at the

TCD
5, 855–883, 2011

glacier summit. We established linear relations between meteorological variables that were simultaneously observed at the glacier summit during 2005–2007, and gridded reanalysis datasets. Based on an energy-mass balance model and estimated meteorological inputs, we calculated the average evaporation for the period 1979–2007, thereby yielding the ideal precipitation ($289 \pm 35\,\mathrm{mm\,yr^{-1}}$) for the present-day glacier geometry. The ideal precipitation is consistent with the long-term average precipitation recorded at the nearby Tien Shan station ($292 \pm 102\,\mathrm{mm\,yr^{-1}}$). This result suggests that the recent dynamics of the glacier have been regulated by the long-term average precipitation. Constrained by the ideal precipitation, the ideal summer mean temperature (June–August) is $-3.85 \pm 0.60\,^{\circ}\mathrm{C}$, as required to maintain the present-day glacier geometry. A reconstructed long-term mass balance, based on climate data from the Tien Shan station, reveals in detail the fluctuations in glacier mass balance over the past 80 yr. Our study fills decadal gaps between remotely sensed images that have been recently utilized to detect changes in glacier extent in the Tien Shan. Although glacier dynamics are not considered in the mass balance reconstruction, we confirmed that the effect on mass-balance and ideal conditions of changing glacier extent is insignificant compared with the calculated uncertainty due to the varying seasonalities of meteorological inputs. This study provides the long-term annual mass balance for the past 80 yr, which are important data as boundary forcing for fluctuations in glacier geometory.

Model validation revealed that the influence on glacier mass balance of a darkened surface due to dust fall should be taken into account (Fig. 5). However, the dust effect is not considered in the long-term mass balance reconstruction. We are currently analysing ice cores retrieved from the summit of the Gregoriev Glacier in 2007. If a relation is established between the concentration of dust particles in the ice core and surface albedo, it will be possible to obtain a more realistic reconstruction of the glacier mass balance. For this calculation, the timing of dust fall has a strong effect on the mass balance (Fujita, 2007). This type of calculation represents an alternative application of the results of ice-core analyses.

TCD
5, 855–883, 2011

If spatially interpolated or extrapolated meteorological inputs are prepared, it is possible to calculate spatial and temporal changes in glacier mass balance over a wider area, thereby filling decadal gaps in glacier fluctuations revealed by remotely sensed data. Because the energy-mass balance model used in this study also outputs glacier runoff, it will be possible to analyse the regional water cycle (e.g., Aizen et al., 2007b; Hagg et al., 2007).

Acknowledgements. We are deeply indebted to B. Moldobekov and C. Reigber (Central Asian Institute for Applied Geosciences) and Top Asia Co. Ltd. (Kyrgyzstan) for logistical support in the field. This study is part of the Ili Projects funded by the Research Institute for Humanity and Nature (Japan), and was supported by a Grant-in-Aid for Scientific Research (No. 19253001) from MEXT, Japan.

References

Adler, R. F., Huffman, G. J., Chang, A., Ferraro, R., Xie, P. P., Janowiak, J., Rudolf, B., Schneider, U., Curtis, S., Bolvin, D., Gruber, A., Susskind, J., Arkin, P., and Nelkin, E.: The version-2 global precipitation climatology project (GPCP) monthly precipitation analysis (1979–present), J. Hydrometeorol., 4(6), 1147–1167, 2003.

Aizen, V. B.: The mass budget of the Golubina Glacier during 1959/60–1981/1982, Data of Glaciol. Studies, Moscow, USSR, 53, 44-45, 1985 (in Russian).

Aizen, V. B., Maximov, N. V., and Solodkov, P. A.: The dynamics of the Goloubin Glacier during the last 20 years, Works SANII, 91(172), 82–87, 1983 (in Russian).

Aizen, V. B., Kuzmichenok, V. A., Surazakov, A. B., and Aizen, E. M.: Glacier changes in the central and northern Tien Shan during the last 140 years based on surface and remote-sensing data, Ann. Glaciol., 43, 202–213, doi:10.3189/172756406781812465, 2006.

Aizen, V. B., Kuzmichenok, V. A., Surazakov, A. B., and Aizen, E. M.: Glacier changes in the Tien Shan as determined from topographic and remotely sensed data, Global Planet. Change, 56, 328–340, doi:10.1016/j.gloplacha.2006.07.016, 2007a.

Aizen, V. B., Aizen, E. M., and Kuzmichenok, V. A.: Glaciers and hydrological changes in the Tien Shan: simulation and prediction, Environ. Res. Lett., 2, 045019, doi:10.1088/1748-9326/2/4/045019, 2007b.

TCD
5, 855–883, 2011

ASTER-GDEM: available at: http://www.gdem.aster.ersdac.or.jp (last access: 12 March 2011), 2009.
Avsuyk, G. A.: Tuyksu glaciers, Hydrometeo Publishing, Leningrad, USSR, 170 pp., 1984 (in Russian).
Bolch, T.: Climate change and glacier retreat in northern Tien Shan (Kazakhstan/Kyrgyzstan) using remote sensing data, Global Planet. Change, 56(1–2), 1–12, doi:10.1016/j.gloplacha.2006.07.009, 2007.
Dyurgerov, M. B.: Glacier mass balance and regime: data of measurements and analysis, Occasional Paper No. 55, Boulder, Colorado, available at: http://instaar.colorado.edu/other/occ_papers.html (last access: 12 March 2011), 2002.
Fujita, K.: Effect of dust event timing on glacier runoff: sensitivity analysis for a Tibetan glacier, Hydrol. Process., 21(21), 2892–2896, doi:10.1002/hyp.6504, 2007.
Fujita, K.: Effect of precipitation seasonality on climatic sensitivity of glacier mass balance, Earth Planet. Sci. Lett., 276(1–2), 14–19, doi:10.1016/j.epsl.2008.08.028, 2008.
Fujita, K. and Ageta, Y.: Effect of summer accumulation on glacier mass balance on the Tibetan Plateau revealed by mass-balance model, J. Glaciol., 46(153), 244–252, doi:10.3189/172756500781832945, 2000.
Fujita, K., Seko, K., Ageta, Y., Pu, J. C., and Yao, T. D.: Superimposed ice in glacier mass balance on the Tibetan Plateau, J. Glaciol., 42(142), 454–460, 1996.
Fujita, K., Ohta, T., and Ageta, Y.: Characteristics and climatic sensitivities of runoff from a cold-type glacier on the Tibetan Plateau, Hydrol. Process., 21(21), 2882–2891, doi:10.1002/hyp.6505, 2007.
Fujita, K., Suzuki, R., Nuimura, T., and Sakai, A.: Performance of ASTER and SRTM DEMs, and their potential for assessing glacial lakes in the Lunana region, Bhutan Himalaya, J. Glaciol., 54(185), 220–228, doi:10.3189/002214308784886162, 2008.
Fujita, K., Sakai, A., Nuimura, T., Yamaguchi, S., and Sharma, R. R.: Recent changes in Imja Glacial Lake and its damming moraine in the Nepal Himalaya revealed by in-situ surveys and multi-temporal ASTER imagery, Environ. Res. Lett., 4, 045205, doi:10.1088/1748-9326/4/4/045205, 2009.
Golubev, G. N.: The Glacier Hydrology, L. Hydrometeoizdat, 246 pp., 1976 (in Russian).
Glazirin, G. E.: Mountain glacial systems, their structure and evolution, Hydrometeo Publishing, Leningrad, USSR, 110 pp., 1991 (in Russian).
Hagg, W. J., Braun, L. N., Uvarov, V. N., and Makarevich, K. G.: A comparison of three meth-

TCD
5, 855–883, 2011

ods of mass balance determination in the Tuyuksu Glacier Region, Tien Shan, J. Glaciol., 50(171), 505–510, doi:10.3189/172756504781829783, 2005.
Hagg, W. J., Braun, L. N., Kuhn, M., and Nesgaard, T. I.: Modelling of hydrological response to climate change in glacierized Central Asian catchments, J. Hydrol., 332(1–2), 40–53, doi:10.1016/j.jhydrol.2006.06.021, 2007.
Jarvis, A., Reuter, H. I., Nelson, A., and Guevara, E.: Hole-filled seamless SRTM data V4, International Centre for Tropical Agriculture (CIAT), available at: http://srtm.csi.cgiar.org/, (last access: 12 March 2011), 2008.
Kalnay, E., Kanamitsu, M., Kistler, R., Collins, W., Deaven, D., Gandin, L., Iredell, M., Saha, S., White, G., Woollen, J., Zhu, Y., Chelliah, M., Ebisuzaki, W., Higgins, W., Janowiak, J., Mo, K. C., Ropelewski, C., Wang, J., Leetmaa, A., Reynolds, R., Jenne, R., and Joseph, D.: The NCEP/NCAR 40-year reanalysis project, Bull. Amer. Meteorol. Soc., 77(3), 437–471, 1996.
Khromova, T. E., Dyurgerov, M. B., and Barry, R. G.: Late-twentieth century changes in glacier extent in the Ak-shirak Range, Central Asia, determined from historical data and ASTER imagery, Geophys. Res. Lett., 30, 1863, doi:10.1029/2003GL017233, 2003.
Konovalov, V. G.: Computation and Forecast of glacier melt in Central Asia, Hydrometeo Publishing, Leningrad, USSR, 230 pp., 1979 (in Russian).
Krenke, A. N.: Mass exchange in glacial systems on the USSR territory, Hydrometeo Publishing, Leningrad, USSR, 287 pp., 1982 (in Russian).
Kutuzov, S. and Shahgedanova, M.: Glacier retreat and climatic variability in the eastern Terskey-Alatoo, inner Tien Shan between the middle of the 19th century and beginning of the 21st century, Global Planet. Change, 69, 59–70, doi:10.1016/j.gloplacha.2009.07.001, 2009.
Nagornov, O., Konovalov, Y., and Mikhalenko, V.: Prediction of thermodynamic state of the Gregoriev ice cap, Tien Shan, central Asia, in the future, Ann. Glaciol., 43, 307–312, doi:10.3189/172756406781812221, 2006.
Narama, C., Shimamura, Y., Nakayama, D., and Abdrakhmatov, K.: Recent changes of glacier coverage in the western Terskey-Alatoo range, Kyrgyz Republic, using Corona and Landsat, Ann. Glaciol., 43, 223–229, doi:10.3189/172756406781812195, 2006.
Surazakov, A. B. and Aizen, V. B.: Estimating volume change of mountain glaciers using SRTM and map-based topographic data, IEEE Trans. Geosci. Remote Sens., 44(10), 2991–2995, 2006.
Surazakov, A. B. and Aizen, V. B.: Positional accuracy evaluation of declassified Hexagon KH-9

TCD
5, 855–883, 2011

mapping camera imagery, Photogramm. Eng. Remote Sens., 76(5), 603–608, 2010.
Suslov, V. F.: Abramov glacier, Hydrometeo Publishing, Leningrad, USSR, 206 pp., 1980 (in Russian).
Thompson, L. G., Mosley-Thompson, E., Davis, M., Lin P. N., Yao, T., Dyurgerov, M., and Dai, J.: "Recent warming": ice core evidence from tropical ice cores with emphasis on Central Asia, Global Planet. Change, 7(1–3), 145–156, doi:10.1016/0921-8181(93)90046-Q, 1993.

TCD
5, 855–883, 2011

Table 1. Parameters for estimating daily meteorological variables (y) at the summit of the Gregoriev Glacier by linear regression ($y = ax + b$) from variables of reanalysis datasets (x). Air temperature and precipitation are preliminarily modified for the Tien Shan station. Also listed is the correlation coefficient (r) and its significance level (p). Regression equations for wind speed and precipitation are obtained by assuming a zero intercept ($b = 0$) to avoid negative wind speed and persistent precipitation.

Variable	a	b	r	$p <$
Air temperature	0.93	−1.61	0.916	0.001
Wind speed	1.37	0.00	0.047	–
Relative humidity	−0.18	79.33	−0.158	0.01
Solar radiation	0.91	42.99	0.812	0.001
Precipitation	1.18	0.00	0.614	0.01

TCD
5, 855–883, 2011

Table 2. Flow components and change in height of stakes around the summit of the Gregoriev Glacier for 2006 and 2007 (except AWS, which was also measured in 2005). dH, dSF, dSA and dVD denote changes in the horizontal position of the stake, vertical change in the glacier surface, snow accumulation obtained from the stake height, and vertical depletion by glacier flow, respectively. The horizontal flow directions are shown in Fig. 3.

Stake	dH ($m\,yr^{-1}$)	dSF (m)	dSA (m)	dVD ($m\,yr^{-1}$)
AWS 2005/06	0.20	−0.25	0.33	−0.52
AWS 2006/07	0.60	0.25	0.79	−0.53
Stake 1	1.12	0.29	1.53	−1.21
Stake 2	0.46	0.28	1.21	−0.91
Stake 3	0.25	0.39	0.96	−0.56
Stake 4	0.44	0.27	1.18	−0.89
Stake 5	0.79	0.16	1.26	−1.07
Stake 6	1.45	−0.07	1.15	−1.19
Old stake	1.96	−0.09	0.35	−0.43

TCD
5, 855–883, 2011

Table 3. Annual net accumulation, precipitation and summer mean temperature required to maintain the present-day geometry of the Gregoriev Glacier. The snow density was measured from three snow pits excavated every year. Evaporation is the average of the model calculation for 29 yr.

Vertical depletion by glacier flow	0.53 ± 0.01 m yr^{-1}
Surface snow density	451 ± 46 kg m^{-3}
Net accumulation	238 ± 27 mm w.e. yr^{-1}
Modelled evaporation	51 ± 8 mm w.e. yr^{-1}
Ideal precipitation	289 ± 35 mm yr^{-1}
Precipitation at Tien Shan station	292 ± 102 mm yr^{-1}
Summer mean air temperature at the glacier summit (4600 m a.s.l.)	-3.06 ± 0.60 °C

TCD
5, 855–883, 2011

Table 4. Specific mass balances (SMB) calculated for the Gregoriev Glacier.

	Duration (days)	SMB (m w.e.)
DGPS survey 2006–2007	373	−0.36
Calculation 2006–2007	373	−0.41
Control calculation 2005–2006	407	−1.34
Dust-run 2005–2006	407	−1.60

TCD
5, 855–883, 2011

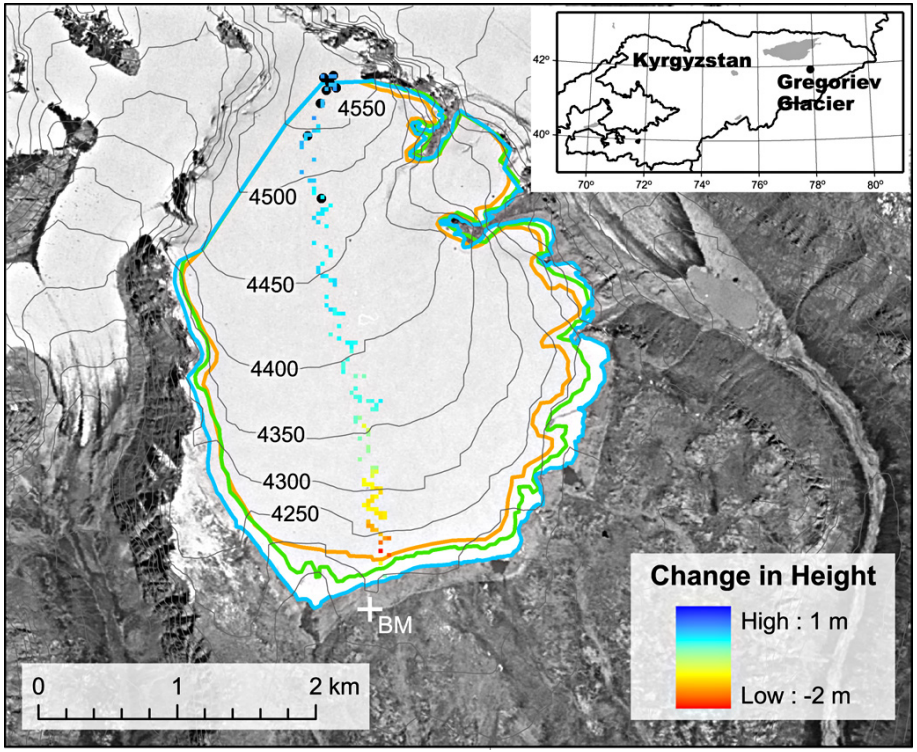

Fig. 1. Location (inset) and satellite image of the Gregoriev Glacier taken by Hexagon KH-9 on 21 August 1980 (Surazakov and Aizen, 2010). Glacier boundaries are manually delineated from satellite images of Hexagon KH-9 (1980, blue) and pan-sharpened Landsat ETM+ (1999, green and 2006, yellow). Contour lines (50-m interval) are drawn based on an SRTM-DEM. The white cross and black dots denote the benchmark for DGPS surveys and mass balance stakes, respectively. Coloured 15-m cells denote changes in elevation, which was averaged from 1-m resolution DEMs obtained by DGPS surveys in July 2006 and August 2007 (see the text for details).

TCD
5, 855–883, 2011

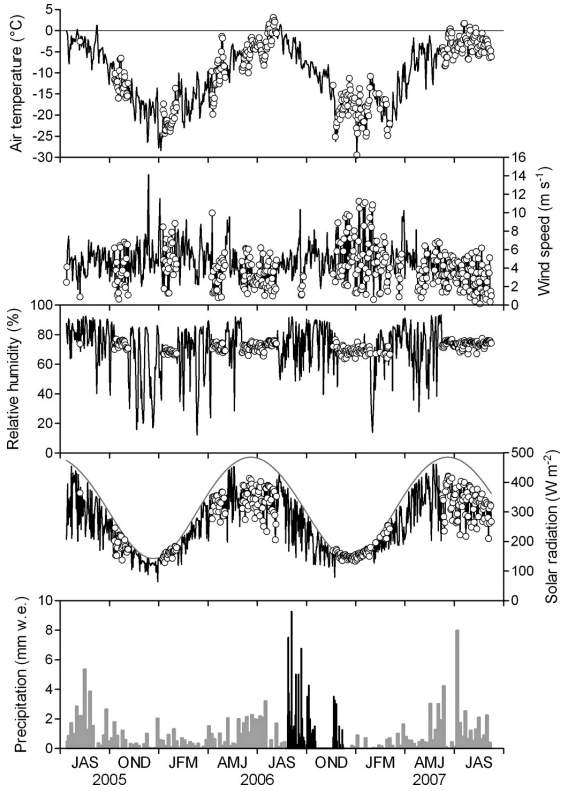

Fig. 2. Meteorological records observed at the summit of the Gregoriev Glacier from July 2005 to September 2007. The upper to lower panels respectively show daily values of air temperature, wind speed, relative humidity, solar radiation, and precipitation. Lines and circles in the panels (except precipitation) indicate observed and estimated variables, respectively. In the lowermost panel (precipitation), black and grey bars represent observed and estimated daily precipitation, respectively. The grey line in the panel showing solar radiation represents the solar irradiance calculated for the top of the atmosphere.

TCD
5, 855–883, 2011

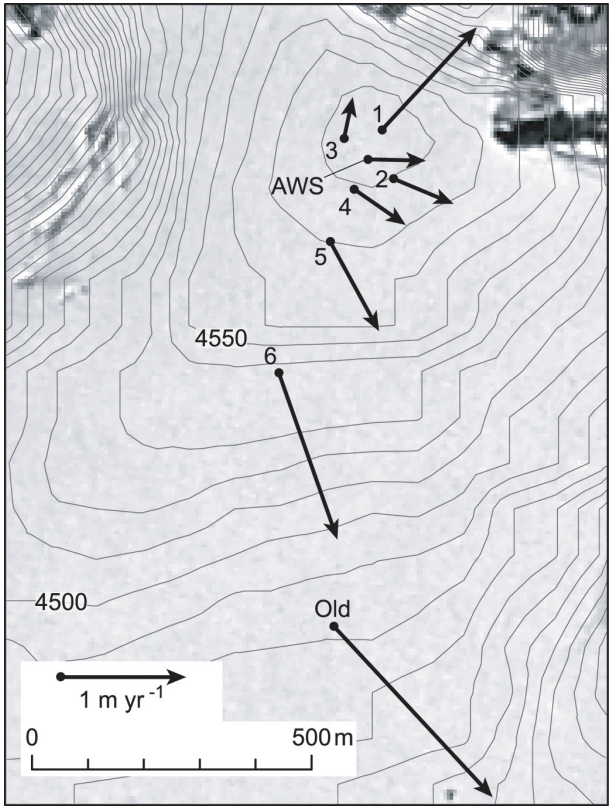

Fig. 3. Surface flow velocities (arrows) measured at stakes (dots) on the Gregoriev Glacier between 2006 and 2007. Contour lines (10-m interval) are drawn based on an SRTM-DEM. The background image is a Hexagon KH-9 image taken on 21 August 1980. Values are summarized in Table 2. AWS, Old and other numbers denote automatic weather station, pre-existing stake and stakes we installed, respectively.

TCD
5, 855–883, 2011

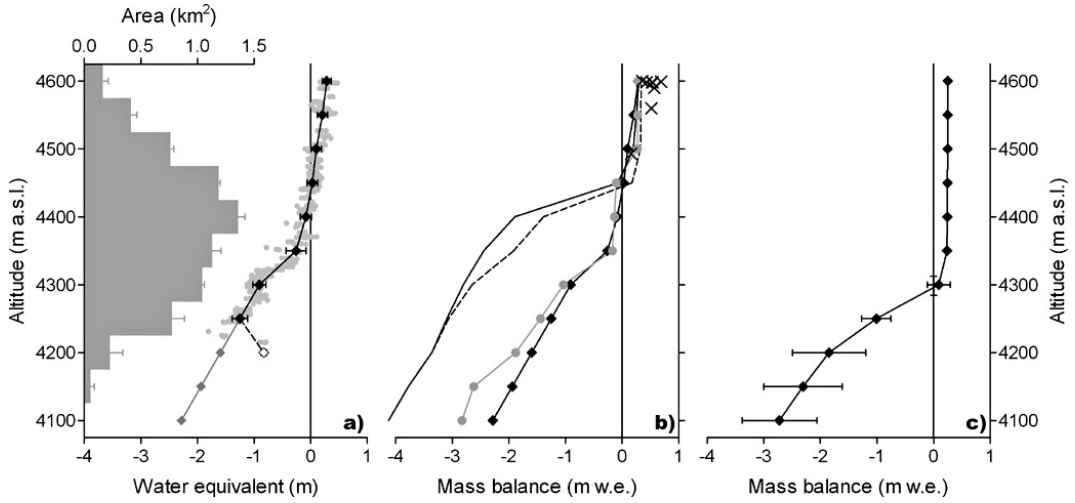

Fig. 4. **(a)** Altitudinal distributions of area and changes in surface elevation for the Gregoriev Glacier between July 2006 and August 2007. **(b)** Mass balance profiles calculated for the period 2005–2007. **(c)** Ideal mass balance profile for the present-day glacier geometry. The area data with error bars in **(a)** are obtained from SRTM and ASTER-GDEM, with the glacier extent delineated from Landsat ETM+ images taken in 1999 and 2006. Grey dots, and black and grey diamonds along the solid line in **(a)** denote changes in a 1-m grid cell, averages at the 50-m altitude band, and extrapolated changes for the unmeasured lower part of the glacier, respectively. The lowest survey point (open diamond) was excluded from the analysis because it probably detected the ground. Black diamonds, grey circles, and solid and broken lines in **(b)** denote DGPS surveys, calculated mass balance profile for the period 2006–2007, and mass balance profiles for the period 2005–2006, for which the albedo reduction is considered (solid line) or not considered (broken line), respectively. Crosses in **(b)** denote the mass balance calculated from changes in stake height and from the average snow density.

TCD
5, 855–883, 2011

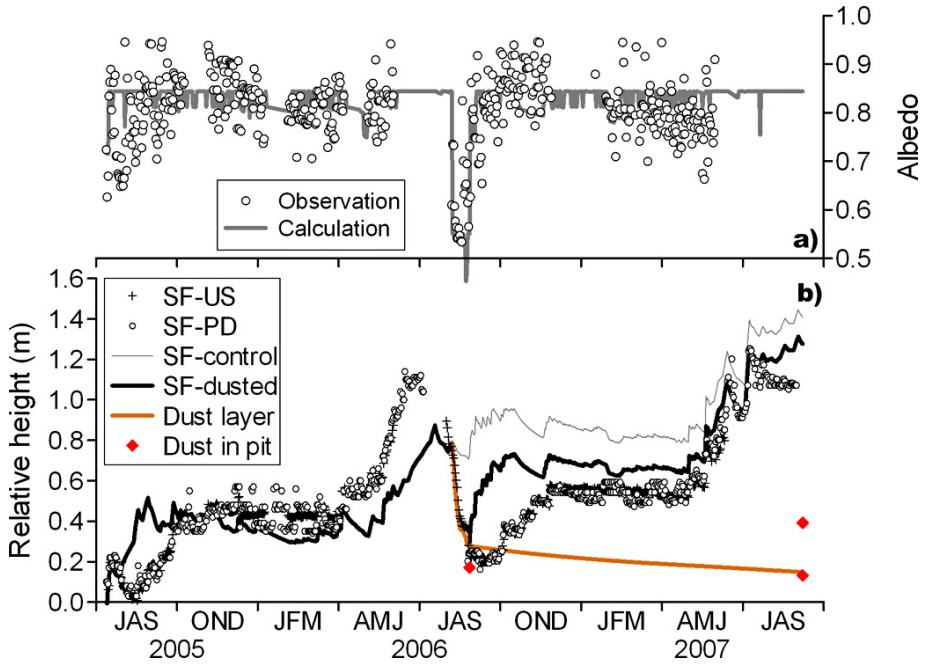

Fig. 5. Albedo **(a)** and relative surface height **(b)** at the summit of the Gregoriev Glacier from July 2005 to September 2007. Circles and the thick grey line in **(a)** denote observed and calculated albedos. Symbols in **(b)** denote surface levels measured by an ultrasonic sensor (crosses, SF-US) and by a photo-diode sensor (circles, SF-PD). Lines in **(b)** denote calculated surface levels in the control run (thin grey line, SF-control), dust run (thick black line, SF-dusted), and the modelled dust layer tracked in the snow layer (thick brown line, Dust layer). The calculated surface levels overlap for the first year. Also shown are the dust layers observed in the snow pits excavated in 2006 and 2007 (red diamonds).

TCD
5, 855–883, 2011

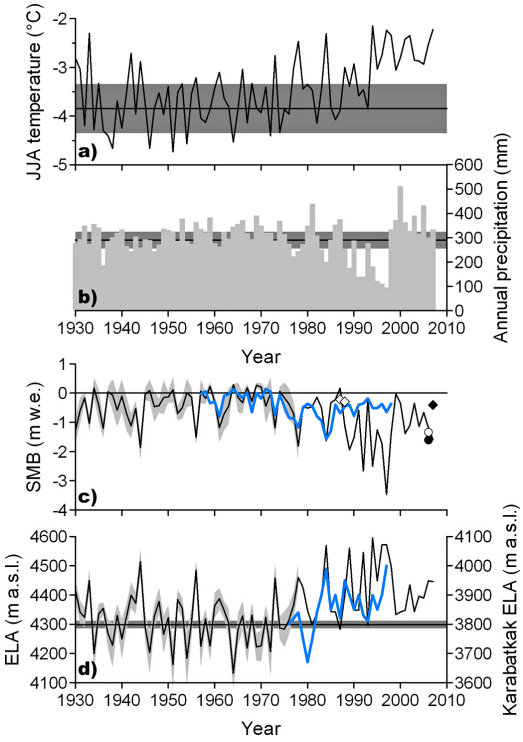

Fig. 6. (a) Summer (JJA) mean air temperature at 4600 m a.s.l., **(b)** annual precipitation, **(c)** calculated specific mass balance (SMB), and **(d)** calculated equilibrium line altitude (ELA) of the Gregoriev Glacier for the past 80 yr. Thick blue lines in **(c)** and **(d)** denote records of the Karabatkak Glacier. Open and solid diamonds in **(c)** denote the observed mass balance of the glacier and the mass balance calculated from DGPS surveys (this study). Open and solid circles in **(c)** denote calculated mass balances for which the dust effect was considered or not considered, respectively. Horizontal lines with dark grey bands denote the ideal variables for the present-day glacier geometry. Light grey shading for the SMB and ELA denotes the standard deviation obtained from different 29 seasonal patterns of meteorological input (1979–2007).

TCD
5, 855–883, 2011